University of Kentucky
UKnowledge

Chemistry Faculty Publications   Chemistry

8-28-2014

Low-Temperature Phase Transitions in a Soluble Oligoacene and Their Effect on Device Performance and Stability

J. W. Ward
Wake Forest University

K. P. Goetz
Wake Forest University

A. Obaid
Wake Forest University

Marcia M. Payne
University of Kentucky, marcia.payne@uky.edu

P. J. Diemer
Wake Forest University

See next page for additional authors

Right click to open a feedback form in a new tab to let us know how this document benefits you.
Follow this and additional works at: https://uknowledge.uky.edu/chemistry_facpub

Part of the Chemistry Commons

Repository Citation

Authors

J. W. Ward, K. P. Goetz, A. Obaid, Marcia M. Payne, P. J. Diemer, C. S. Day, John E. Anthony, and O. D. Jurchescu

Low-Temperature Phase Transitions in a Soluble Oligoacene and Their Effect on Device Performance and Stability

Low-temperature phase transitions in a soluble oligoacene and their effect on device performance and stability

J. W. Ward,[1] K. P. Goetz,[1] A. Obaid,[1] M. M. Payne,[2] P. J. Diemer,[1] C. S. Day,[3] J. E. Anthony,[2] and O. D. Jurchescu[1,a)]

[1]Department of Physics, Wake Forest University, Winston-Salem, North Carolina 27109, USA
[2]Department of Chemistry, University of Kentucky, Lexington, Kentucky 40506, USA
[3]Department of Chemistry, Wake Forest University, Winston-Salem, North Carolina 27109, USA

The use of organic semiconductors in high-performance organic field-effect transistors requires a thorough understanding of the effects that processing conditions, thermal, and bias-stress history have on device operation. Here, we evaluate the temperature dependence of the electrical properties of transistors fabricated with 2,8-difluoro-5,11-bis(triethylsilylethynyl)anthradithiophene, a material that has attracted much attention recently due to its exceptional electrical properties. We have discovered a phase transition at $T = 205\,\mathrm{K}$ and discuss its implications on device performance and stability. We examined the impact of this low-temperature phase transition on the thermodynamic, electrical, and structural properties of both single crystals and thin films of this material. Our results show that while the changes to the crystal structure are reversible, the induced thermal stress yields irreversible degradation of the devices. © 2014 AIP Publishing LLC.
[http://dx.doi.org/10.1063/1.4894238]

Soluble small-molecule organic semiconductors exhibit excellent electrical performance when crystallized by a variety of techniques; these include ink-jet printing,[1,2] polymer blends,[3,4] solution shearing,[5] vibration assisted crystallization (VAC),[6] and spray deposition.[7–10] Charge transport in these materials is strongly dependent on the crystal packing motif, which is dictated by the molecular structure: very subtle modifications in the chemistry of the compound yield significant changes in the electronic couplings[11,12] and device performance.[3,6,10,13–15] In addition, such systems are susceptible to variations in crystalline structure upon processing. The existence of more than one possible crystal structure for a compound is referred to as polymorphism, a phenomenon that is quite common in molecular crystals given the weak nature of the intermolecular interactions that are characteristic to such systems.[5,16–28] With 5,11-bis(triethylsilylethynyl)anthradithiophene (TES ADT), for example, the solvent type used during film deposition affects its crystalline structure and morphology and alters its field-effect mobility by over one order of magnitude.[29] In the same material, polymorphism can be driven by post-processing steps such as solvent annealing[30] or by sweeping the temperature.[31] The fluorinated version of the aforementioned compound, 2,8-difluoro-TES ADT (diF-TES ADT), also exhibits temperature-dependent polymorphism.[32] In this system, an enantiotropic phase transition was reported near room temperature, which affected its electrical properties, and the observed changes were completely reversible. In the present study, we explore the properties of this material over a broader temperature range and discover the presence of another structural phase transition present at $T = 205\,\mathrm{K}$. This transition is completely reversible in terms of crystalline

structure, but it yields irreversible deterioration of the electrical performance in organic thin-film transistors (OTFTs) fabricated from this material. The transition was studied using differential scanning calorimetry (DSC), X-ray diffraction (XRD), and OTFT measurements. This study provides a complete phase diagram of the phases present in diF-TES ADT in the temperature range of 120–350 K and their effect on charge transport and device stability.

DSC measurements were performed in hermetically sealed aluminum pans at a scanning rate of 20 K/min using a Q2000 TA Instruments differential scanning calorimeter. Multiple heat/cool sweeps were performed over the 180–350 K temperature range. Temperature-dependent XRD was carried out in order to elucidate the structural changes within the material as it passed through the phase transitions. Single crystal XRD measurements were not successful as the crystal routinely cracked or shattered upon cooling below 280 K, preventing the collection of sufficient data to determine the crystalline structure at temperatures below the 205 K transition. We were, however, able to gain qualitative information about the low-temperature phase by performing powder XRD. Powder diffraction was acquired on a Bruker D8 DaVinci diffractometer with Cu-K$_\alpha$ radiation and a liquid nitrogen-cooled low-temperature stage fitted with a Be hemispherical enclosure. The source beam was conditioned using a 0.1 mm lateral slit and 2.5° Soller slits. The reflected beam was conditioned with a 0.6 mm lateral slit, 2.5° Soller slits, and a Ni filter to remove K$_\beta$ contributions. The powder was lightly mechanically ground and sifted using a fine mesh filter screen to ensure an even coating on a zero-background Si substrate. After initial measurements were taken at room temperature ($T = 294\,\mathrm{K}$), the powder was sequentially cooled to $T = 200\,\mathrm{K}$, then $T = 150\,\mathrm{K}$, and finally returned to $T = 294\,\mathrm{K}$, all at a rate of 5 K/min. Scan data sets were collected at each temperature for the range $10° < 2\theta < 40°$.

a)Author to whom correspondence should be addressed. Electronic mail: jurchescu@wfu.edu.

The device studies were carried out using bottom-gate, bottom-contact field-effect transistor (FET) structures with heavily doped n^{++}Si as the gate electrode and 200 nm SiO$_2$ gate dielectric. The source and drain contacts were defined by photolithography and lift-off, with Ti (5 nm)/Au (45 nm) deposited using e-beam evaporation. The substrates were cleaned with hot acetone and hot isopropanol followed by UV-ozone exposure and an ethanol rinse. A self-assembled monolayer (SAM) treatment was performed on the electrodes by soaking the substrate in a 30 mM room-temperature bath of pentafluorobenzenethiol (PFBT) (Sigma Aldrich) for 30 min followed by a 5 min sonication in ethanol. The organic semiconductor was spin-coated from a 1.2 wt.% chlorobenzene (Sigma Aldrich) solution at 1000 rpm. As-prepared devices were placed in vacuum for at least 24 h prior to measurement to ensure full solvent removal. Electrical characterization was carried out during cooling, followed by heating using an Agilent 4155C Semiconductor Parameter Analyzer in combination with LakeShore cryogenic probestation. The heating/cooling rates were 5 K/min to prevent film cracking.

Figure 1 depicts the DSC results obtained for a typical diF-TES ADT sample. Two peaks can be clearly distinguished, denoting the presence of two distinct transitions separated by a $\Delta T = 90$ K interval. The known room-temperature phase transition manifests itself as a peak at $T = 294$ K, characterized by a latent heat of $\Delta H = 1.8$ kJ/mol, in agreement with previous reports.[32] Further cooling shows an additional peak at $T = 205$ K, with latent heat twice as large at $\Delta H = 3.6$ kJ/mol. Both transitions appear to be enantiotropic in nature. For the remainder of this article, the individual phases will be denoted from warmest to coolest as α, β, and γ. Slight shifts in the peak positions are observed during the heating segments of the DSC, but the temperature interval between the two peaks remains constant.

The devices operate as p-type FETs, and in Figure 2(a) we present a typical device characteristics in the saturation regime (with drain-source voltage, $V_{DS} = -40$ V). We extracted the mobility μ from the slope of the square root of the drain current (I_D) vs the gate voltage (V_{GS}) using the current-voltage relationship

$$I_\mathrm{D} = \frac{W}{L}\frac{C_\mathrm{i}}{2}\mu(V_\mathrm{GS} - V_\mathrm{th})^2, \tag{1}$$

where W and L are the channel width and length, respectively, C_i is the gate oxide capacitance per unit area, and V_th is the threshold voltage of the device. The plot in Figure 2(a) corresponds to T = 295 K, and representative transfer characteristics at different temperatures are displayed in Figure SI1 for the saturation and linear regimes, respectively.[33] The evolution of the FET mobility, as characterized in the saturation regime of operation, versus temperature is shown in Fig. 2(b). We measured more than 15 devices, and all showed similar behavior. This plot shows several inflection points at temperatures that coincide with peak locations in the DSC measurements. For this reason, we attribute them to the phase transitions. A similar trend was observed in data extracted from the linear regime (Figure SI2); however, to minimize the effects due to the contacts and to more effectively access the intrinsic properties of the material, our discussion will be limited to the saturation regime characterization.[33] The change in the slope of the μ vs. T plot begins at $T = 294$ K, marking the transition from the α-phase into a region where the α- and β-phases co-exist, in agreement with previous results.[32] In the temperature range of $220\,\mathrm{K} < T < 275\,\mathrm{K}$, the mobility varies monotonically with temperature and the film consists of pure β-phase. Upon further cooling, the onset of a region in which the mobility increases is observed. This marks a phase-coexistence region between the β- and γ-phases, with the β-phase gradually being converted into the higher mobility γ-phase. At $T < 175$ K, the film consists of a single phase, i.e., the γ-phase. Small differences in the transition temperatures between the DSC and electrical measurements are due to the differences in the grain size between the organic semiconductor powder used in the DSC measurements and the thin-films used in the organic FET (OFET) characterization. Other causes for peak shifting in DSC measurements are variations in heating and cooling rates and the total mass of the sample, though the peak onset remains the same. In addition, the width of the transition windows varied slightly between measurements on different samples, which is typical for transitions that proceed via a nucleation and growth mechanism.[34]

Each of the three phases exhibits activated behavior in the evolution of the mobility with temperature, as observed in Fig. 2. We extracted the activation energies E_A from the Arrhenius relationship given by Eq. (2) (see the inset in Fig. 2(b)) for the temperature zones where only pure phases are present

$$\mu = \mu_0 e^{-E_\mathrm{A}/(k_\mathrm{B}T)}, \tag{2}$$

where μ_0 is the trap-free mobility and k_B is the Boltzmann constant. The corresponding values for each phase are $E_\mathrm{A}(\alpha) = 20$ meV, $E_\mathrm{A}(\beta) = 115$ meV, and $E_\mathrm{A}(\gamma) = 40$ meV. The electrical properties are completely reversible when the system contains α and/or β polymorphs, but they cannot be recovered upon heating once the devices reach the γ-phase, as the mobility drops irreversibly (Figure SI3).[33] This result can be better understood upon a closer look at Figure 3, which shows pictures of a diF-TES ADT single crystal while passing through the two transition points. The high temperature transition (α- to β-phases) does not induce any notable optical changes within the crystal (Figs. 3(a) and 3(b)), but
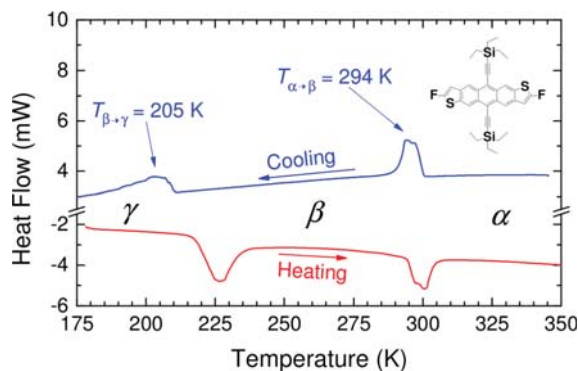

FIG. 1. DSC spectrum of diF-TES ADT displaying the presence of two phase transitions at $T = 294$ K and $T = 205$ K. The heating (bottom, red) and cooling (top, blue) curves are shown and phases are defined as α, β, and γ. The inset shows the molecular structure of diF-TES ADT.
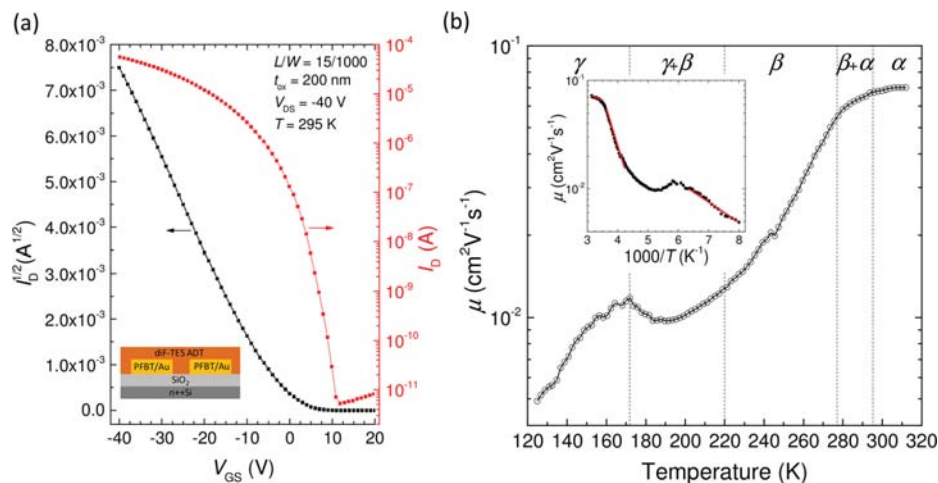
FIG. 2. (a) Typical current-voltage characteristics for a device in the saturation regime of operation ($V_{DS} = -40$ V), taken at $T = 295$ K. This device has a geometry of $W = 1000\,\mu$m and $L = 15\,\mu$m. The inset displays the schematic of the device that was used. (b) Evolution of the saturation field-effect mobility (μ) with temperature. The inflection points correspond to the structural phase transitions. Individual phases are identified by α, β, and γ. The inset shows representative slopes used in the activation energy calculation.

as the crystal transitions into the γ-phase, it changes color from red to a pale pink, exhibits cracking, and in some cases shatters completely. This behavior suggests that in spite of the fact that the 205 K transition is enantiotropic in nature, as pointed out by our DSC measurements, the mechanical stress associated with this transformation induces irreversible damage to the crystal. This explains the degradation in our transistor measurements and highlights the detrimental effect of such transition in the reliability of devices made on this material when measured at low temperatures. The β to γ transition is thus very different than the one observed near room temperature, which resulted in minor, reversible changes in the electrical characteristics.[32] Encouragingly, the characteristic transition temperature is well below the device operating temperatures, and while the transition degrades the device performance, it does not pose a threat for the operation of diF-TES ADT OTFTs in opto-electronic applications. This is unlike the case of 6,13-bis(triisopropylsilylethynyl)

pentacene, where such dramatic transitions occur slightly above room temperature, yielding film cracking and irreversible performance degradation.[35,36]

Because the single crystals cracked when cooled into the γ-phase, we were not able to determine the crystal structure of the new polymorph. Nevertheless, our temperature-dependent powder XRD measurements (Figure 4) clearly show that the transition observed at low temperature is structural in nature, and that the phase transformation occurs gradually, with the β and γ polymorphs co-existing over a temperature interval that vary slightly from sample to sample. The two room-temperature measurements taken before (red) and after (not shown) the cooling are very similar, confirming the fact that the transition is reversible. Measurements taken near the transition temperature (150 K and 200 K) exhibit noticeably different spectrums beyond simple shifts in the peak positions, which are also significantly different from those observed near room temperature. Based on the mobility data presented in Fig. 2(b), the spectrum taken at $T = 200$ K corresponds to a phase-coexistence region between β and γ polymorphs, while at $T = 150$ K, a single phase (γ) is present.
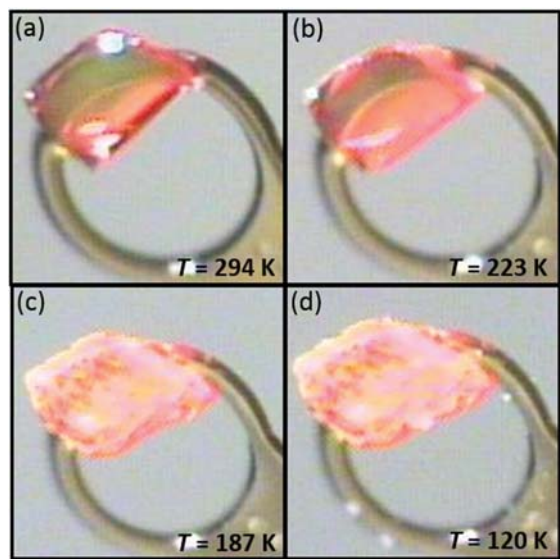

FIG. 3. Optical micrograph of a diF-TES ADT single crystal at (a) $T = 294$ K, (b) $T = 223$ K, (c) $T = 187$ K, and (d) $T = 120$ K. Cooling of the material at a rate of 5 K/min shows both a change in color from red (a) to pink (b) and the onset of internal cracking and segmentation of the crystal (c) and (d). The return to room temperature resulted in further degradation of the crystal.
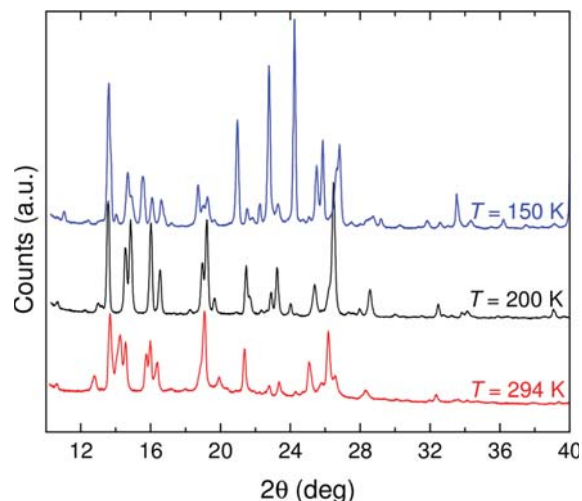

FIG. 4. Powder diffraction of diF-TES ADT at $T = 294$ K (red), $T = 200$ K (black), and $T = 150$ K (blue). Dissimilar patterns indicate a structural change within the material.
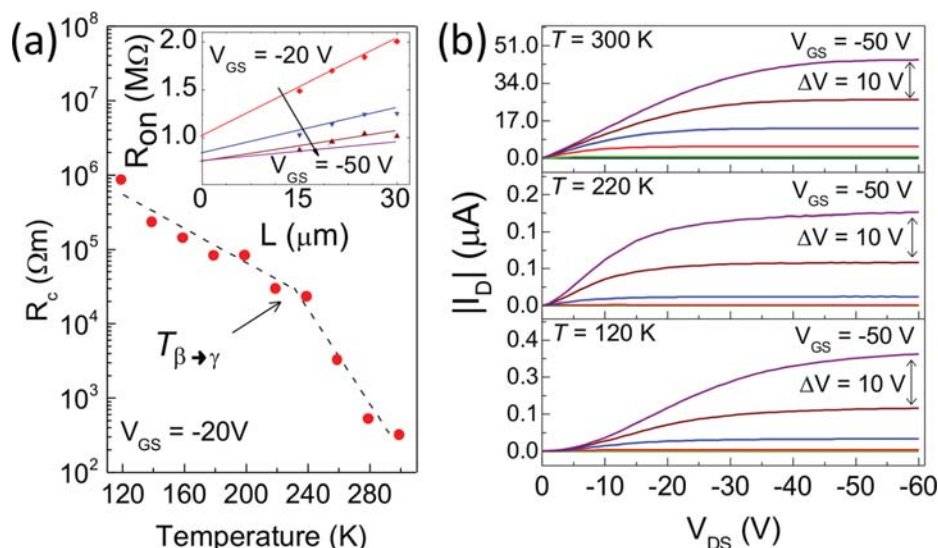
FIG. 5. (a) Evolution of the contact resistance with temperature for $V_{GS} = -20$ V. The inflections indicate the impact that structural changes in the semiconducting material have on the injection of charges between the SAM-treated device electrodes and diF-TES ADT. In the inset, representative curves for the total device resistance as a function of channel length are shown for several gate voltages. (b) Output characteristics of the same device characterized in the α-phase ($T = 300$ K), β-phase ($T = 220$ K), and γ-phase ($T = 120$ K).

The observed changes in the device mobility reported in Fig. 2(b) have two possible origins. First, the intrinsic material mobility varies as a result of the different molecular packing characteristic to each of the three polymorphs, promoting different electronic structures.[11] Second, the changes in the crystalline packing at the surface of the electrode occurring when the system undergoes the transition cause shifts in the position of the highest occupied molecular orbital (HOMO) level of the semiconductor. This alters the Schottky barrier at the injecting contact, and thus the contact resistance. We have previously shown that a shift of $\sim$0.2 eV in HOMO is obtained by transitioning from a pure (001) to a mixed (111):(001) orientation with respect to the surface, with no changes in the crystalline structure. This resulted in variation of the contact resistance (R_c) by more than two orders of magnitude.[37] It is therefore expected that similar or greater shifts will occur in the case of a polymorph transition. To investigate the effect of the structural phase transition on the contact resistance of our OTFTs, we analyzed it as a function of temperature using the gated transmission line method (TLM). For a set of devices of different channel lengths and fixed widths, we measured the total device resistance in the linear regime of operation

$$R_{on} = \partial I_D / \partial V_{DS}, \tag{3}$$

where $R_{on} = 2R_c + R_{channel}$.[38] Plotting the values of R_{on} as a function of channel length for each gate-source voltage V_{GS} and extrapolating the total resistance to $L = 0$ allowed us to extract the contact resistance of the FET (see the inset in Figure 5(a)). In Figure 5(a), we show the evolution of R_c as a function of temperature for $V_{GS} = -20$ V. Typical output curves used for these calculations are shown in Figure 5(b). The increase in the contact resistance with decreasing temperature is typical for OFETs and is observed as more pronounced deviations from linearity in the low V_{DS} region (Figure 5(b)). Systems in which the semiconductor undergoes no phase transition exhibit an exponential dependence of R_c on temperature.[39] Nevertheless, in our measurements, we also observe an inflection point of the R_c vs. T curve as a result of the conversion of the β to γ polymorphs, in agreement with our hypothesis that the changes in the crystal

packing induce shifts in the HOMO level. Studies are ongoing to describe in detail the impact of the transition on the band structure of diF-TES ADT.

In conclusion, we have shown that (2,8-difluoro-5,11-bis(triethylsilylethynyl) anthradithiophene) undergoes a low-temperature phase transformation at $T = 205$ K. We discovered a new phase, which we define as the γ polymorph. This phase exhibits higher mobility in OTFTs, in spite of the significantly higher contact resistance that results from an unfavorable shift in the HOMO level. The phase transition is completely reversible in XRD and DSC measurements, but once the system undergoes the changes, the device performance cannot be recovered. We believe this effect results from the strain induced in the crystal upon the molecular rearrangement, which yields cracks within the film. Our results provide a complete picture of the structure-property relationships as a function of temperature in a high performance organic semiconductor and highlight the impact that fine adjustments in crystalline packing can have on the overall device performance and operational stability.

[1]H. Minemawari, T. Yamada, H. Matsui, J. Tsutsumi, S. Haas, R. Chiba, R. Kumai, and T. Hasegawa, Nature **475**, 364 (2011).
[2]T. N. Ng, S. Sambandan, R. Lujan, A. C. Arias, C. R. Newman, H. Yan, and A. Facchetti, Appl. Phys. Lett. **94**, 233307 (2009).
[3]K. P. Goetz, Z. Li, J. W. Ward, C. Bougher, J. Rivnay, J. Smith, B. R. Conrad, S. R. Parkin, T. D. Anthopoulos, A. Salleo, J. E. Anthony, and O. D. Jurchescu, Adv. Mater. **23**, 3698 (2011).
[4]R. Hamilton, J. Smith, S. Ogier, M. Heeney, J. E. Anthony, I. McCulloch, J. Veres, D. D. C. Bradley, and T. D. Anthopoulos, Adv. Mater. **21**, 1166 (2009).
[5]G. Giri, E. Verploegen, S. C. B. Mannsfeld, S. Atahan-Evrenk, D. H. Kim, S. Y. Lee, H. A. Becerril, A. Aspuru-Guzik, M. F. Toney, and Z. Bao, Nature **480**, 504 (2011).
[6]P. J. Diemer, C. R. Lyle, Y. Mei, C. Sutton, M. M. Payne, J. E. Anthony, V. Coropceanu, J.-L. Brédas, and O. D. Jurchescu, Adv. Mater. **25**, 6956 (2013).

[7]M. Aleksandrova, G. Dobrikov, I. Zhivkov, B. Kyosev, and T. Dobreva, J. Optoelectron. Adv. Mater. **11**, 1400 (2009).

[8]K. X. Steirer, M. O. Reese, B. L. Rupert, N. Kopidakis, D. C. Olson, R. T. Collins, and D. S. Ginley, Sol. Energy Mater. Sol. Cells **93**, 447 (2009).

[9]N. A. Azarova, J. W. Owen, C. A. Mclellan, M. A. Grimminger, E. K. Chapman, J. E. Anthony, and O. D. Jurchescu, Org. Electron. **11**, 1960 (2010).

[10]Y. Mei, M. A. Loth, M. Payne, W. Zhang, J. Smith, C. S. Day, S. R. Parkin, M. Heeney, I. McCulloch, T. D. Anthopoulos, J. E. Anthony, and O. D. Jurchescu, Adv. Mater. **25**, 4352 (2013).

[11]V. Coropceanu, J. Cornil, D. A. da Silva Filho, Y. Olivier, R. Silbey, and J.-L. Brédas, Chem. Rev. **107**, 926 (2007).

[12]J.-L. Brédas, D. Beljonne, V. Coropceanu, and J. Cornil, Chem. Rev. **104**, 4971 (2004).

[13]H. Dong, X. Fu, J. Liu, Z. Wang, and W. Hu, Adv. Mater. **25**, 6158 (2013).

[14]J. E. Anthony, A. Facchetti, M. Heeney, S. R. Marder, and X. Zhan, Adv. Mater. **22**, 3876 (2010).

[15]J. W. Ward, R. Li, A. Obaid, M. M. Payne, D.-M. Smilgies, J. E. Anthony, A. Amassian, and O. D. Jurchescu, Adv. Funct. Mater. **24**, 5052 (2014).

[16]V. Podzorov, E. Menard, A. Borissov, V. Kiryukhin, J. A. Rogers, and M. E. Gershenson, Phys. Rev. Lett. **93**, 086602 (2004).

[17]J. Chen, J. Anthony, and D. C. Martin, J. Phys. Chem. B **110**, 16397 (2006).

[18]O. D. Jurchescu, A. Meetsma, and T. T. M. Palstra, Acta Crystallogr., Sect. B: Struct. Sci. **62**, 330 (2006).

[19]L. Antolini, G. Horowitz, F. Kouki, and F. Garnier, Adv. Mater. **10**, 382 (1998).

[20]C. Avendano, Z. Zhang, A. Ota, H. Zhao, and K. R. Dunbar, Angew. Chem., Int. Ed. Engl. **50**, 6543 (2011).

[21]T. Siegrist, C. Kloc, J. H. Schön, B. Batlogg, R. C. Haddon, S. Berg, and G. A. Thomas, Angew. Chem., Int. Ed. Engl. **40**, 1732 (2001).

[22]C. C. Mattheus, A. B. Dros, J. Baas, A. Meetsma, J. L. de Boer, and T. T. M. Palstra, Acta Crystallogr., Sect. C: Cryst. Struct. Commun. **57**, 939 (2001).

[23]A. Brillante, I. Bilotti, F. Biscarini, R. G. Della Valle, and E. Venuti, Chem. Phys. **328**, 125 (2006).

[24]M. Campione, S. Tavazzi, M. Moret, and W. Porzio, J. Appl. Phys. **101**, 083512 (2007).

[25]P. Hermet, J.-L. Bantignies, A. Rahmani, J.-L. Sauvajol, and M. R. Johnson, J. Phys. Chem. A **109**, 4202 (2005).

[26]H. Pan, P. Liu, Y. Li, Y. Wu, B. S. Ong, S. Zhu, and G. Xu, Adv. Mater. **19**, 3240 (2007).

[27]D. J. Gundlach, T. N. Jackson, D. G. Schlom, and S. F. Nelson, Appl. Phys. Lett. **74**, 3302 (1999).

[28]M. Mas-Torrent and C. Rovira, Chem. Rev. **111**, 4833 (2011).

[29]J. Chen, M. Shao, K. Xiao, A. J. Rondinone, Y.-L. Loo, P. R. C. Kent, B. G. Sumpter, D. Li, J. K. Keum, P. J. Diemer, J. E. Anthony, O. D. Jurchescu, and J. Huang, Nanoscale **6**, 449 (2014).

[30]K. C. Dickey, J. E. Anthony, and Y.-L. Loo, Adv. Mater. **18**, 1721 (2006).

[31]L. Yu, X. Li, E. Pavlica, F. P. V. Koch, G. Portale, I. da Silva, M. A. Loth, J. E. Anthony, P. Smith, G. Bratina, B. K. C. Kjellander, C. W. M. Bastiaansen, D. J. Broer, G. H. Gelinck, and N. Stingelin, Chem. Mater. **25**, 1823 (2013).

[32]O. D. Jurchescu, D. Mourey, S. Subramanian, S. R. Parkin, B. M. Vogel, J. E. Anthony, T. N. Jackson, and D. J. Gundlach, Phys. Rev. B **80**, 085201 (2009).

[33]See supplementary material at http://dx.doi.org/10.1063/1.4894238 for additional temperature dependant properties of diF-TES ADT.

[34]F. H. Herbstein, Acta Crystallogr., Sect. B: Struct. Sci. **62**, 341 (2006).

[35]J.-H. Bae, H. Kim, G. Horowitz, and S.-D. Lee, Solid-State Electron. **63**, 163 (2011).

[36]J. Chen, C. K. Tee, J. Yang, C. Shaw, M. Shtein, J. Anthony, and D. C. Martin, J. Polym. Sci., Part B: Polym. Phys. **44**, 3631 (2006).

[37]J. W. Ward, M. A. Loth, R. J. Kline, M. Coll, C. Ocal, J. E. Anthony, and O. D. Jurchescu, J. Mater. Chem. **22**, 19047 (2012).

[38]S. M. Baier, M. S. Shur, K. Lee, N. C. Cirillo, Jr., and S. A. Hanka, IEEE Trans. Electron Devices **32**, 2824 (1985).

[39]B. H. Hamadani and D. Natelson, Appl. Phys. Lett. **84**, 443 (2004).